

Localisation, looping and pop-out in rod-like structures

G.H.M. van der Heijden

Centre for Nonlinear Dynamics, Civil Engineering Building, University College London,
Gower Street, London WC1E 6BT, UK (g.heijden@ucl.ac.uk)

Keywords: clamped Cosserat rod, localisation, self-contact, bifurcation, loop pop-out, plied structure

Abstract. Long slender structures such as textile yarns and ocean cables show localised buckling behaviour under torsional loading. In a 1D elastic theory these localised solutions are described by homoclinic orbits in a dynamical system in which arclength along the structure is the independent variable. Upon continued loading after localisation a snap into self-contact and looping may occur. We discuss the intricate bifurcation behaviour that unfolds after the initial jump and also consider the problem of loop pop-out. We also briefly consider the mechanics of the plied structure that forms and show that the problem is governed by the equations for an elastic rod constrained to lie on a cylinder. This work is relevant for supercoiling DNA molecules and staple fibre yarns.

Introduction

Long thin structures under torsional loading are well known to undergo localised deformation. If the applied tension is insufficiently high the structure (a cable or wire) may ‘throw a loop’. In many applications loop formation is undesirable. In marine cables, if tension is reapplied after looping this may or may not cause the loop to pop out. As the loop is tightened the cable may undergo plastic deformation to an extent that it is permanently damaged. In textile yarns the formation of loops (here often called snarls) during spinning may lead to yarn breakage and a costly waste of time as well as to non-uniformities in the final fabric.

Coyne [3] studied cable looping and pop-out by using the homoclinic solution which describes localised deformation in an infinitely long rod. Here we use an exact formulation for a self-contacting clamped finite-length incompressible circular tube obeying the Kirchhoff equations for a linearly elastic inextensible and unshearable rod. The contact force is obtained numerically as part of the solution of the equilibrium equations and pop-out is inferred when the contact force drops to zero. Multiple points of contact are allowed and we find a bifurcation sequence in which the rod jumps to states of increasing number of self-contacts as a control parameter (end rotation or end shortening) is increased. In the highly twisted case the final configuration is a plied structure known, for instance, from DNA supercoiling [2] and textile yarn twisting [4]. This process of ply formation, although remarkably delicate in its theoretical detail, can easily be observed in a rubber rod. The beginning of ply formation can be seen in Fig. 6. The fully fledged ply has line contact and we show that its mechanics can be idealised as a pair of rods winding around a cylinder.

Formulation of a clamped rod

Consider a thin elastic rod of length L held by end forces and moments. If we denote the position of the rod’s centreline by the vector function \mathbf{R} , then the internal force, \mathbf{F} , and moment, \mathbf{M} , in an element of the rod are governed by the balance equations [1]

$$\mathbf{F}' = \mathbf{0}, \tag{1}$$

$$\mathbf{M}' + \mathbf{r}' \times \mathbf{F} = \mathbf{0}, \tag{2}$$

where $(\)' = d/ds$, s being the arclength parameter measured along the centreline of the rod. We assume the rod to be perfect (i.e., intrinsically straight and untwisted), inextensible and unshearable.

In order to describe fully an equilibrium configuration of the rod we must specify the position of three orthonormal axes $\{\mathbf{d}_1, \mathbf{d}_2, \mathbf{d}_3\}$ as a function of s . Since the rod is inextensible we can choose \mathbf{d}_3 to be the tangent to the centreline of the rod,

$$\mathbf{r}' = \mathbf{d}_3, \quad (3)$$

and \mathbf{d}_1 and \mathbf{d}_2 two vectors in the normal cross-section coincident with the principal bending axes. The evolution of this moving co-ordinate frame along the rod is then governed by

$$\mathbf{d}'_i = \mathbf{u} \times \mathbf{d}_i \quad (i = 1, 2, 3). \quad (4)$$

Here \mathbf{u} is the generalised strain vector whose components in the moving frame are the curvatures ($u_i = \mathbf{u} \cdot \mathbf{d}_i$, $i = 1, 2$) and the twist ($u_3 = \mathbf{u} \cdot \mathbf{d}_3$). We introduce linear constitutive relations between the moments and the strains:

$$\mathbf{M} \cdot \mathbf{d}_1 = B_1 u_1, \quad \mathbf{M} \cdot \mathbf{d}_2 = B_2 u_2, \quad \mathbf{M} \cdot \mathbf{d}_3 = C u_3. \quad (5)$$

B_1 and B_2 are the principal bending stiffnesses about \mathbf{d}_1 and \mathbf{d}_2 , respectively, while C is the torsional stiffness about \mathbf{d}_3 . We shall consider transversely isotropic rods, i.e., we take $B_1 = B_2 = B$.

By integrating the force and moment equations (the latter giving $\mathbf{M} + \mathbf{r} \times \mathbf{F} = \mathbf{M}_0$) and making use of the constitutive relations we obtain the following system of equations:

$$\begin{aligned} \mathbf{r}' &= \mathbf{d}_3, \\ B \mathbf{d}'_3 &= (\mathbf{F} \times \mathbf{r} + \mathbf{M}_0) \times \mathbf{d}_3, \\ B \mathbf{d}'_1 &= (\mathbf{F} \times \mathbf{r} + \mathbf{M}_0) \times \mathbf{d}_1 + (B - C) u_3 \mathbf{d}_3 \times \mathbf{d}_1, \end{aligned} \quad (6)$$

where \mathbf{F} and \mathbf{M}_0 are integration constants and the twist u_3 is also constant in this isotropic case. The third equation has been added because we consider displacement-controlled boundary conditions in which the material vector \mathbf{d}_1 is fixed at the ends. It can be shown that free (i.e., non-self-contacting) solutions subject to clamped boundary conditions are symmetric [7]. It is therefore advantageous to choose the origin of arclength at the middle of the rod. We consider the following clamped boundary conditions:

$$\begin{aligned} \mathbf{R}(-L/2) &= (x(-L/2), y(-L/2), z(-L/2)) = (0, 0, 0), & \mathbf{R}(L/2) &= (0, 0, L - D), \\ \mathbf{d}_3(-L/2) &= (d_{3x}(-L/2), d_{3y}(-L/2), d_{3z}(-L/2)) = (0, 0, 1), & \mathbf{d}_3(L/2) &= (0, 0, *), \\ \mathbf{d}_1(-L/2) &= (d_{1x}(-L/2), d_{1y}(-L/2), d_{1z}(-L/2)) = (1, 0, 0), & \mathbf{d}_1(L/2) &= (\cos R, *, *), \end{aligned} \quad (7)$$

where components have been expressed relative to an orthonormal co-ordinate frame $\{\mathbf{i}, \mathbf{j}, \mathbf{k}\}$ fixed in space and the star signifies that there is no condition on the corresponding component. In a fully displacement-controlled situation we specify the end shortening D and relative end rotation R so that we have 15 conditions for 9 equations and the 6 free parameters $(\mathbf{F}, \mathbf{M}_0)$. Alternatively, we can specify, e.g., the axial end force $F_z = \mathbf{F} \cdot \mathbf{k}$ or the end twisting moment $C u_3 = \mathbf{M}(L/2) \cdot \mathbf{d}_3(L/2) = \mathbf{M}(L/2) \cdot \mathbf{k} = \mathbf{M}_0 \cdot \mathbf{k} = M_{0z}$ and treat D or R as free parameters. Note that the end rotation in (7) is only defined modulo 2π , but that its correct value can be obtained by continuity. More details on the numerical solution of the equations can be found in [7].

Phase-plane analysis – localisation

In the isotropic case the system of equations (6) is completely integrable (i.e., solvable in closed form) and it is instructive to consider the reduced planar system that can be obtained in terms of the angle θ between the tangent and the applied force ($\mathbf{F} \cdot \mathbf{d}_3 = T \cos \theta$, with T is the applied tension):

$$B\theta'' + \frac{M^2}{B} \frac{\sin \theta}{(1 + \cos \theta)^2} - T \sin \theta = 0, \quad (8)$$

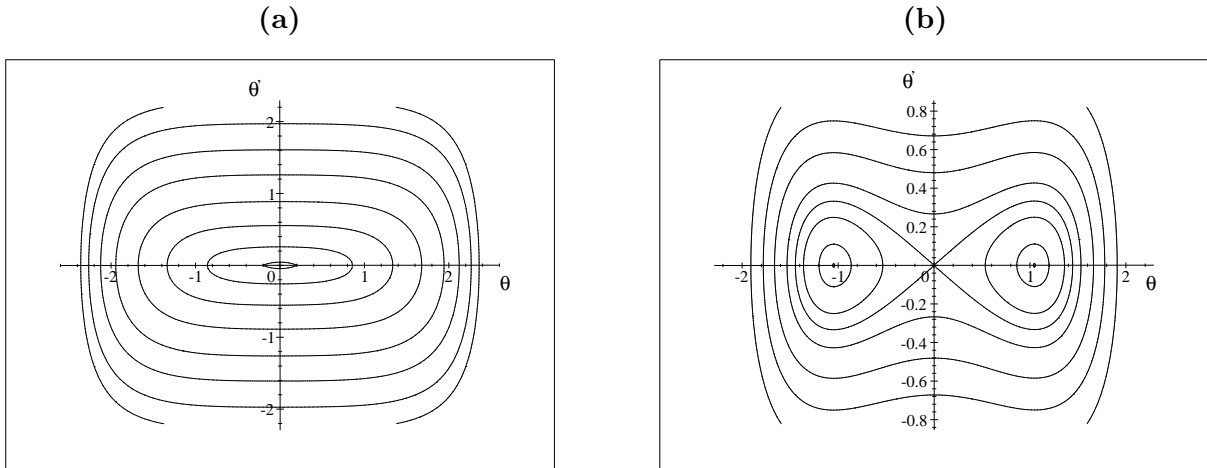


Figure 1: Typical phase portraits for the planar system (8): (a) $M^2 > 4BT$, (b) $M^2 < 4BT$.



Figure 2: Localised rod configuration corresponding to the homoclinic orbits in Fig. 1(b).

where $M = \mathbf{M} \cdot \mathbf{d}_3$ is the applied (axial) moment (details can be found in [8]). This equation for θ is the well-known equation for the inclination angle of the Lagrange top (Kirchhoff's dynamic analogy [1]). The torsional buckling condition (for an infinitely long rod) is given by $M^2 = 4BT$, at which point a pitchfork bifurcation occurs. Phase portraits are depicted in Fig. 1. The portrait for $M^2 < 4BT$ in Fig. 1(b) has a symmetric pair of homoclinic orbits that describe localised deformations of the rod. The fixed points correspond to helical solutions (or the straight rod if $\theta = 0$).

For very long structures the (localised) homoclinic solution (shown in Fig. 2) will be the energetically favourable one, and clamped finite-length solutions will lie close to the homoclinic orbit in the phase plane.

Formulation of a rod with point contacts

Jump conditions. Experience tells us that under high torsional load the rod may jump into self-contact, creating an almost planar loop. Self-contact can be taken into account on the level of 1D rod theory by considering an impenetrable elastic tube of certain radius about the centreline of the rod [7]. In this section we consider configurations with isolated contacts. A contact point is a (single) point in space at which the boundaries of two non-neighbouring (circular) cross-sections meet. We assume that the forces the two cross-sections exert on each other are reactive forces normal to the surface of the rod (i.e., we assume the self-contact to be frictionless). Consequently, the (constant) internal force \mathbf{F} will undergo a discontinuous change. The moment \mathbf{M} , on the other hand, will be assumed to be continuous (i.e., no concentrated moments), as will be \mathbf{R} and the directors \mathbf{d}_i (and hence u_3). From equation (2) we see that in order to ensure continuity of \mathbf{M} across a point of contact, \mathbf{M}_0 will have to change.

We formulate the problem of a self-contacting rod by using the equations for a free rod between contact points and deriving jump conditions to match the solutions at arclength parameters $(s_1, s_2,$

etc.) were contact occurs. Thus we consider the equations (6) with subscripts and write

$$\begin{aligned} \mathbf{r}' &= \mathbf{d}_3, \\ B \mathbf{d}'_3 &= (\mathbf{F}_i \times \mathbf{r} + \mathbf{M}_{i0}) \times \mathbf{d}_3, \\ B \mathbf{d}'_1 &= (\mathbf{F}_i \times \mathbf{r} + \mathbf{M}_{i0}) \times \mathbf{d}_1 + (B - C) u_3 \mathbf{d}_3 \times \mathbf{d}_1. \end{aligned} \quad (9)$$

Here \mathbf{F}_i and \mathbf{M}_{i0} are the as yet unknown constant internal force and matching moment in the section $[s_i, s_{i+1}]$, where $s_0 = 0$, $s_{n+1} = L/2$, and n is the number of contacts. We shall only consider the natural case of solutions with symmetric contacts, i.e., with sections at points $\mathbf{r}(-s)$ and $\mathbf{r}(s)$ touching. At the first point of contact, s_1 , we have the geometrical relations

$$|\mathbf{r}(s_1) - \mathbf{r}(-s_1)| = 2\rho, \quad (10)$$

$$(\mathbf{r}(s_1) - \mathbf{r}(-s_1)) \cdot \mathbf{d}_3(\pm s_1) = 0, \quad (11)$$

where ρ is the radius of the rod. Since \mathbf{F} is defined to be the force from the element at s' acting on the element at s , where $s' > s$, we have

$$\mathbf{F}_0 = \mathbf{F}_1 + \frac{\Delta F_1}{2\rho} (\mathbf{r}(s_1) - \mathbf{r}(-s_1)), \quad (12)$$

where the contact force, of magnitude ΔF_1 , points from $s = -s_1$ to $s = s_1$. For \mathbf{M} to be continuous we need

$$\mathbf{M}(s_1) = \mathbf{F}_0 \times \mathbf{r}(s_1) + \mathbf{M}_{00} = \mathbf{F}_1 \times \mathbf{r}(s_1) + \mathbf{M}_{10}, \quad (13)$$

which, upon using (12), can be rewritten as

$$\mathbf{M}_{10} = \mathbf{M}_{00} + \frac{\Delta F_1}{2\rho} \mathbf{r}(s_1) \times \mathbf{r}(-s_1). \quad (14)$$

The same can be done at each contact and we obtain

$$\mathbf{F}_i = \mathbf{F}_{i-1} - \frac{\Delta F_i}{2\rho} (\mathbf{r}(s_i) - \mathbf{r}(-s_i)), \quad (15)$$

$$\mathbf{M}_{i0} = \mathbf{M}_{(i-1)0} + \frac{\Delta F_i}{2\rho} \mathbf{r}(s_i) \times \mathbf{r}(-s_i) \quad (16)$$

for the constants to be used in (9). These jump conditions give two extra equations for the two unknowns ΔF_i and s_i for each contact-free section of rod.

Our approach to compute branches of self-contacting solutions is as follows. Along a free-rod loading path we monitor the symmetric self-distance defined by

$$\Delta(s) = \sqrt{[x(s) - x(-s)]^2 + [y(s) - y(-s)]^2 + [z(s) - z(-s)]^2}, \quad (17)$$

and when contact first occurs, detected by the condition $\Delta(\bar{s}) = 2\rho$ for some \bar{s} , we use a shooting method to solve the contact equations (9) subject to (15) and (16) with $n = 1$, $s_1 = \bar{s}$ and $\Delta F_1 = 0$. We then use numerical continuation to follow the solution as a loading parameter (D or R) is varied, until the next self-contact is detected and an additional set of equations is solved. Physically acceptable solutions will have $\Delta F_i \geq 0$.

Numerical results. We take $C/B = 5/7$ (corresponding to a Poisson ratio of 0.4) and $\rho/L = 0.03/(2\pi)$. Results for fixed end rotation are shown in Fig. 3. It is found that for R less than about 4.8π the rod delocalises under increasing end shortening D with the 1-contact solution approaching the ring. For R larger than about 4.8π curves in the D - F_z diagram form limit points in D . Physically, the loop starts to rotate and the rod writhes up into a ply. Note that the 1-contact solution goes into compression before it becomes unstable at the fold and jumps into a state with more contacts. Diamonds along the unstable branches indicate where self-penetration ($\Delta < 2\rho$) starts to occur. No bifurcating branch of solutions could be detected, but the numerical approach of this self-penetration

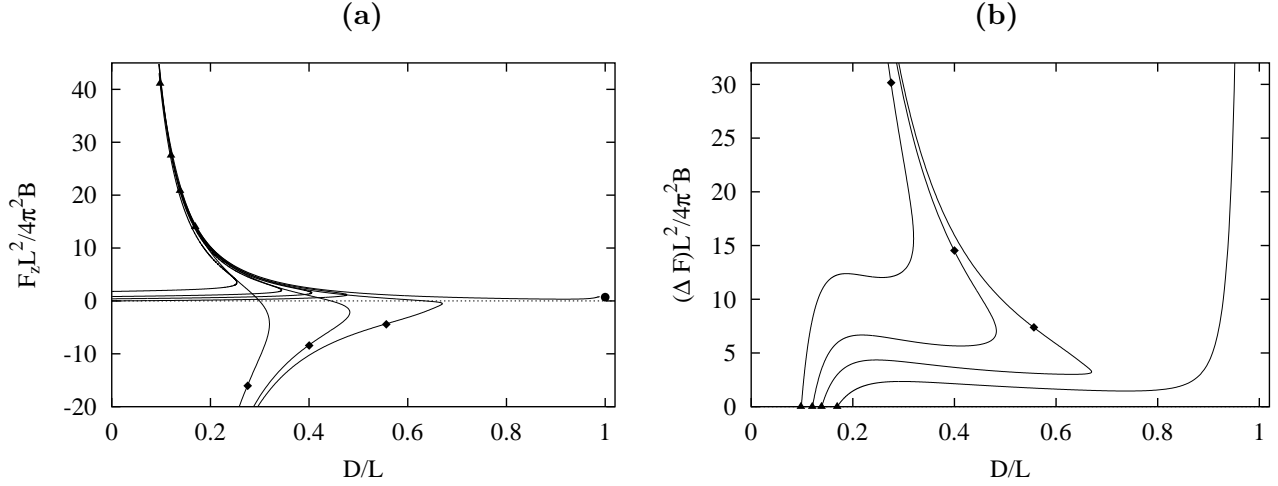


Figure 3: Writhing a rod or not, by varying D/L and fixing R at 4π , 5π , 6π and 8π . For $R = 4\pi$ the rod does not writhe and the curve of 1-point contacts runs up to the ring at $D/L = 1$ (indicated by the circle). In contrast, the curves for $R = 5\pi$, 6π and 8π form limit points, signifying that the rod writhes up into a ply. The transition to writhing takes place between $R = 4.8\pi$ and $R = 5\pi$. Triangles indicate pop-out points where ΔF drops to zero (see (b)) and self-contact is lost. Diamonds indicate points where, presumably, an interval of self-contact is formed. ($C/B = 5/7$, $\rho/L = 0.03/(2\pi)$.)

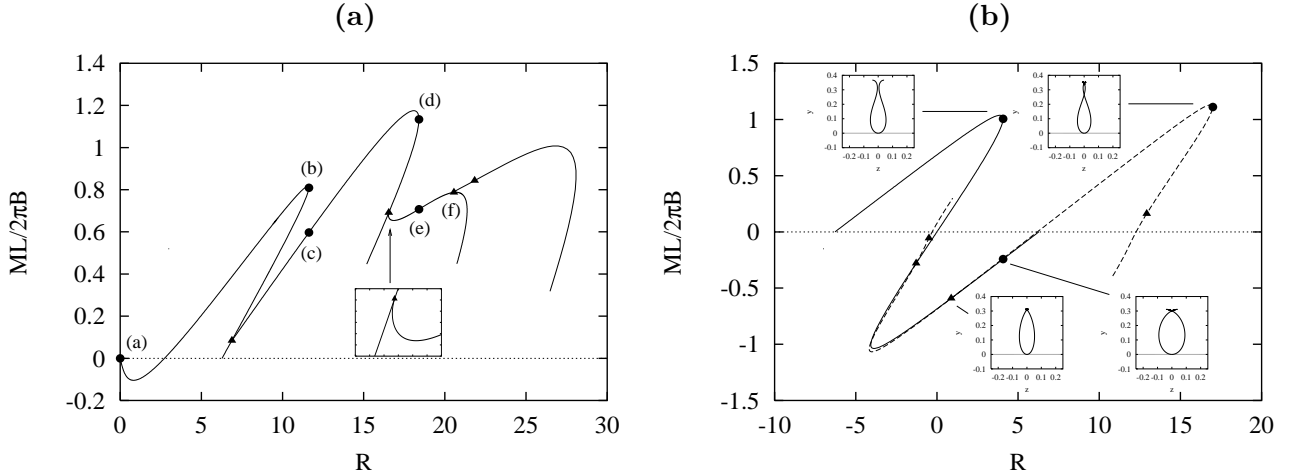


Figure 4: Ply formation under varying R and (a) $D/L = 0.5$, (b) $D/L = 0.86$. All the lower branches coming in at the various folds are unstable. Triangles indicate pop-out points where one self-contact is lost/gained. In (a) curves for up to three points of self-contact are included. Labels refer to the 3D shapes shown in Fig. 6, while the inset shows that the 2-contact curve forms a limit point to the left. In (b) the dashed curve is for 1-contact solutions. Insets give true z - y views of the rod's centreline at the indicated points. ($C/B = 5/7$, $\rho/L = 0.03/(2\pi)$.)

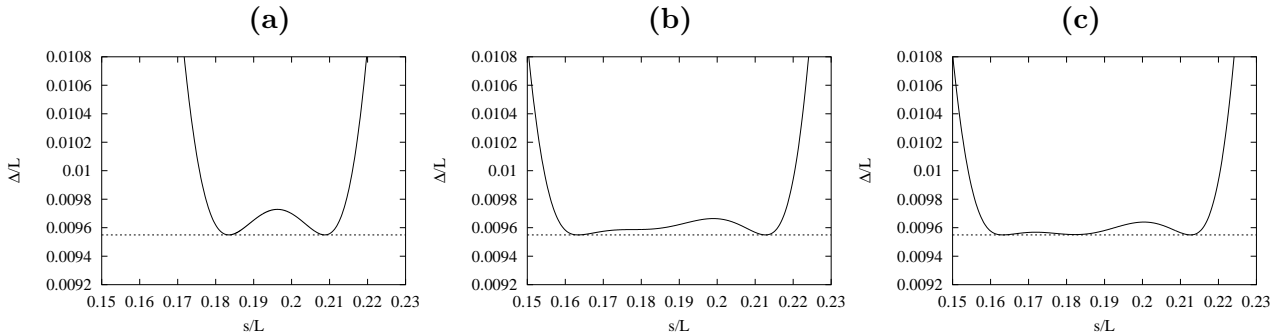


Figure 5: Self-distance Δ against arclength illustrating the formation of the third point of contact along the 2-contact branch in Fig. 4(a). The minimum possible value of Δ is 2ρ , attained at self-contact, and is indicated by the dotted horizontal lines. The right-most self-contact turns out to have the largest pressure force ΔF . ($C/B = 5/7$, $\rho/L = 0.03/(2\pi)$.)

suggests that a branch of solutions with an interval of self-contacts might bifurcate. This is different from the constant- D case discussed below where a branch of 2-contact solutions bifurcates off the 1-contact branch. Fig. 3(b) shows how the contact force ΔF varies with D .

Results for fixed end shortening are shown in Figs 4, 5 and 6. In Fig. 4(a), for $D/L = 0.5$, we find solutions with up to 3 points of self-contact. The transition from the contact-free to the 1-contact, and the transition from the 1-contact to the 2-contact solution, are through dynamic jumps at folds, while the transition from 2-contact to 3-contact is smooth. True-view 3D shapes of the rod at these events are shown in Fig. 6. Extensive numerical searches did not give any hint of the existence of a branch of 4-contact solutions as R is increased further. This is consistent with the work of Coleman & Swigon [2] who find, for closed rods, that at some point the third self-contact grows into an interval of self-contacts, still flanked by two points of self-contact. Fig. 5 illustrates the formation of the third point of contact along the 2-contact branch in Fig. 4(a) using the symmetric self-distance $\Delta(s)$ to monitor the process. It reveals that the third contact is formed between the two existing contacts.

Fig. 4(b) shows that for $D/L = 0.86$ multistability occurs: at the fold along the (solid) contact-free curve the rod can either snap-through and remain without self-contacts, or jump into a configuration with one point of self-contact. (Of course, we cannot rule out the existence of further stable solutions.) Experiments reveal that the contact-free option is normally taken. In fact, the 1-contact curve goes round a fold and intersects the free rod curve a second time at $R = -1.2841$ where again ΔF drops to zero. This ‘pop-out’ only involves unstable branches. Upon increase of D/L the two pop-out points coalesce at $D/L = 0.8946$, leaving a contact curve disconnected from the contact-free curve.

Loop pop-out. If the looped rod has residual twist, i.e., if $R > 2\pi$, then at the point of self-contact a force will act to maintain the contact. If the end shortening is decreased by pulling the ends (keeping R fixed) the loop will be tightened up to a point where the loop pops open. This pop-out only occurs in rods of finite thickness; an infinitely thin rod with $R > 2\pi$ would not go unstable and could be pulled out straight. In many practical cases a cable or pipe will kink (i.e., suffer plastic deformation) before pop-out is reached, damaging the structure.

Pop-out may also occur in rods with multiple points of self-contact when one contact point is lost (as in Fig. 4(a)). At the point of pop-out (out of a single contact) the shape of the rod is again governed by the contact-free rod equations. Therefore, in the numerical continuations which produced Fig. 3 we can infer pop-out when the self-distance Δ reaches 2ρ . The locus of pop-out points thus obtained is shown by the solid curve in Fig. 7 on which some R -values are highlighted. Along a 1-point contact curve in Fig. 3 pop-out is defined by the intersection point of this curve with the free rod curve at the same value of R . At this point the force ΔF drops to zero (see Fig. 3(b)). For a rod of zero radius pop-out is described mathematically by a pitchfork bifurcation; at finite radius it becomes a type of discontinuous bifurcation.

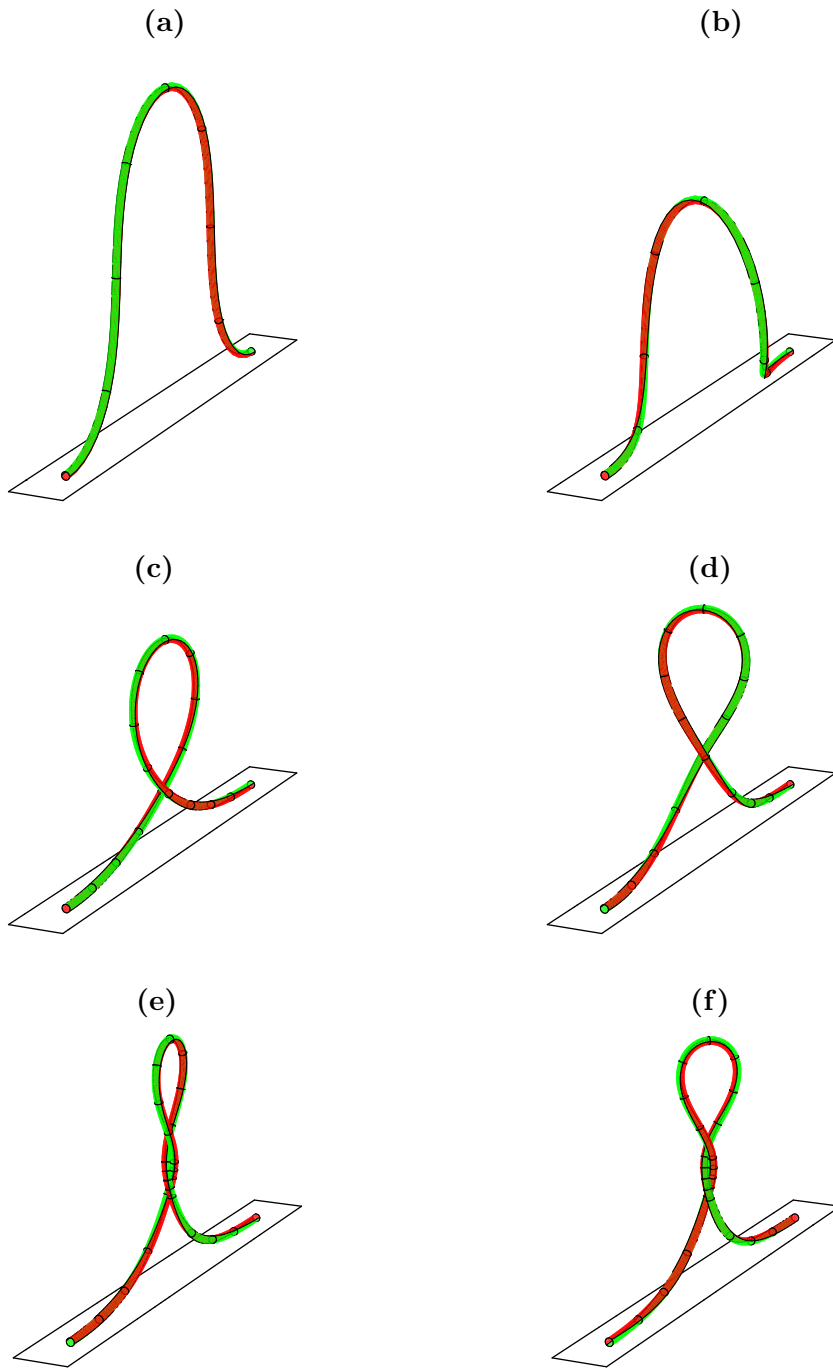


Figure 6: True 3D views of the rod along stable solution paths in Fig. 4(a). Labels correspond to the labels in that figure. The starting point (a) is at the planar elastica. The first jump, into 1-point contact (from (b) to (c)), occurs at $R = 11.6315$; the second jump, into 2-point contact (from (d) to (e)), occurs at $R = 18.4027$. The transition to 3-point contact at (f) (corresponding to (c) in Fig. 5) is smooth.

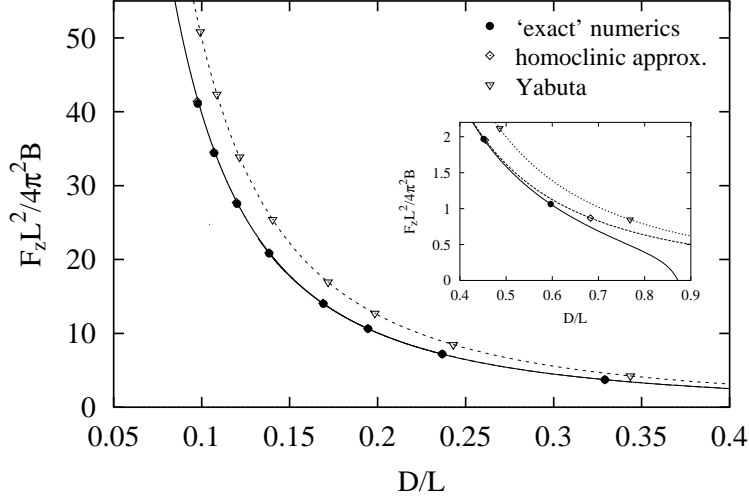


Figure 7: Pop-out locus parametrised by R . Markers are for $R = 2.5\pi, 3\pi, 3.5\pi, 4\pi, 5\pi, 6\pi, 7\pi$ and 8π (in increasing order of tension). The solid curve is obtained from our criterion $\Delta = 2\rho$, the long dashed curve represents results based on the homoclinic orbit, while the short dashed curve shows Yabuta’s approximation. The inset shows further results with markers for $R = 2.25\pi$ and $R = 2.1\pi$. For $R = 2.25\pi$ and higher the homoclinic results are very accurate. ($C/B = 5/7$, $\rho/L = 0.03/(2\pi)$.)

A semi-analytical estimate of the conditions at pop-out can be obtained by following (and slightly improving upon) Coyne [3] in using the homoclinic solution of the rod equations. For this homoclinic solution the shape of the rod is given by (see, e.g., [11])

$$\begin{aligned}
 x(s) &= \frac{1}{F_z} \sqrt{4BF_z - M_z^2} \operatorname{sech} \left(\frac{s}{2B} \sqrt{4BF_z - M_z^2} \right) \sin \left(\frac{M_z s}{2B} \right), \\
 y(s) &= -\frac{1}{F_z} \sqrt{4BF_z - M_z^2} \operatorname{sech} \left(\frac{s}{2B} \sqrt{4BF_z - M_z^2} \right) \cos \left(\frac{M_z s}{2B} \right), \\
 z(s) &= s - \frac{1}{F_z} \sqrt{4BF_z - M_z^2} \tanh \left(\frac{s}{2B} \sqrt{4BF_z - M_z^2} \right),
 \end{aligned} \tag{18}$$

with the self-contact occurring at arclength $s = \bar{s}$ such that

$$z(\bar{s}) = 0, \quad x(\bar{s}) = \rho. \tag{19}$$

Further, in [8] the expressions

$$D = (2/F_z) \sqrt{4BF_z - M_z^2} \quad \text{and} \quad R = \frac{M_z L}{C} + 4 \arccos \left(\frac{M_z}{2\sqrt{BF_z}} \right) \tag{20}$$

are derived for the end shortening and end rotation of the homoclinic solution. From (18)–(20) we can find the tension and end shortening at pop-out as a function of the radius of the rod, ρ , and the amount of end rotation, R , applied. The result is the long dashed curve in Fig. 7. Also included in the diagram is the highly idealised result (giving $F_z = 2\pi^2 B/D^2$) of Yabuta et al. [12] (taking $u_3 = (R - 2\pi)/L$ for the residual twist) who assume one turn of a circular helix as the shape of the loop and a perfectly straight rod elsewhere.

It is seen that for $R > 2.25\pi$ the results based on the homoclinic approximation are virtually indistinguishable from the ‘exact’ numerical results. Notice that the pop-out curve (in fact any of the three curves in Fig. 7) considered as a whole is independent of the stiffness ratio C/B ; its parametrisation by R , of course, does depend on this ratio.

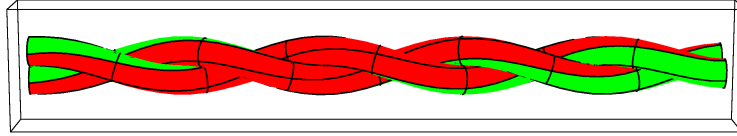


Figure 8: Example of a non-uniform clamped ply solution.

Depending on whether the 1-contact branch emanates from an unstable or stable branch of contact-free solutions, at pop-out the rod undergoes either a dynamic jump or a smooth transition out of contact. The former is the case in Fig. 3(a) where the rod jumps to a contact-free state at much lower tension (or possibly compression) F_z described by the point vertically down from the pop-out point on the same constant- R curve. Note from Fig. 3(b) that ΔF goes through a maximum before it rapidly drops to zero and pop-out occurs. An alternative way of jumping out of contact is provided by the small-scale limit point seen along the 2-contact branch in Fig. 4(a): if one were to decrease R along this branch the rod would jump out of 2-point contact before the force ΔF dropped to zero.

An example of smooth pop-out is seen in Fig. 4(b).

Rods contacting along an interval – plied structures

The natural progression of the writhing process described in the previous section is to interval contact. In this section we assume that the contact curve is a (segment of a) straight line. The rod forms a ply, by which we shall mean two strands of isotropic rod of circular cross-section winding around a straight line segment of mutual contact, one strand providing a pressure force to a 180-degrees rotated copy of itself. The ply is loaded by end forces and moments which are equivalent to an axial force F (positive for tension) and an axial twisting moment M .

The equilibrium equation for the case of a non-uniform ply was derived in [9]:

$$B\theta'' = \frac{2B}{\rho^2} \sin^3 \theta \cos \theta + \frac{\tau C}{\rho} \cos 2\theta + \frac{F}{2} \sin \theta - \frac{M}{2\rho} \cos \theta, \quad (21)$$

where ρ is the radius of the rod. θ is again the angle between the local tangent to the rod and the applied force (and the contact line). The equation is a special case of the equation for a rod deforming on a cylinder, namely a cylinder of radius equal to the radius of the rod [5]. A solution subject to clamped boundary conditions ($\theta(0) = \theta(L) = 0$, where L is now the length of each of the two strands in the ply) is given in Fig. 8. The ply is very nearly uniform except near the clamped ends. The contact force can be obtained from the balance equations as [6]

$$p = \left(C\tau - \frac{3B}{\rho} \sin \theta \cos \theta \right) \left[\frac{2}{\rho^2} \sin^3 \theta \cos \theta + \frac{C\tau}{B\rho} \cos 2\theta - \frac{M}{2B\rho} \cos \theta + \frac{F}{2B} \sin \theta \right] + \frac{M}{2\rho^2} \sin \theta - \frac{B}{\rho^3} \sin^4 \theta - \frac{C\tau}{\rho^2} \sin \theta \cos \theta - \frac{3B}{\rho} \theta'^2 \cos 2\theta. \quad (22)$$

Note that only the last term is due to the non-uniformity of the ply.

Conclusion

We have considered in detail the bifurcation sequence involved in the onset of plying in clamped rods, and also presented a model for an idealised fully developed ply consisting of two strands winding around each other. The latter model could be solved in conjunction with the point contact equations, subject to appropriate matching conditions, when, as in Fig. 4(a), the contact force in 3-point contact drops to zero and, presumably, line contact is initiated. This was done to describe supercoiling of DNA plasmids (closed pieces of DNA) in [2]. In [10] the present formulation for point and interval

contact was used to estimate the torsional stiffness of DNA molecules by comparison of the numerical results with data obtained from single-molecule experiments.

It is good to remember that this approach assumes the configuration of the ply, in particular the shape of the contact curve. It would be of significant interest to develop a more general ply theory that could also describe bent plies.

References

- [1] S.S. Antman, *Nonlinear Problems of Elasticity* (Springer-Verlag, Berlin, 1995).
- [2] B.D. Coleman & D. Swigon, Theory of supercoiled elastic rings with self-contact and its application to DNA plasmids, *J. Elasticity* **60**, 173-221 (2000).
- [3] J. Coyne, Analysis of the formation and elimination of loops in twisted cable, *IEEE J. Ocean. Eng.* **15**, 72-83 (1990).
- [4] W.B. Fraser & D.M. Stump, The equilibrium of the convergence point in two-strand yarn plying, *Int. J. Solids Struct.* **35**, 285-298 (1998).
- [5] G.H.M. van der Heijden, The static deformation of a twisted elastic rod constrained to lie on a cylinder, *Proc. R. Soc. Lond. A* **457**, 695-715 (2001).
- [6] G.H.M. van der Heijden, A two-strand ply hanging under its own weight, *Nonlinear Dynamics* **43**, 197-208 (2006).
- [7] G.H.M. van der Heijden, S. Neukirch, V.G.A. Goss, J.M.T. Thompson, Instability and self-contact phenomena in the writhing of clamped rods, *International Journal of Mechanical Sciences* **45**, 161-196 (2003).
- [8] G.H.M. van der Heijden & J.M.T. Thompson, Helical and localised buckling in twisted rods: a unified analysis of the symmetric case, *Nonlinear Dynamics* **21**, 71-99 (2000).
- [9] G.H.M. van der Heijden, J.M.T. Thompson, S. Neukirch, A variational approach to loaded ply structures, *Journal of Vibration and Control* **9**, 175-185 (2003).
- [10] S. Neukirch, Extracting DNA twist rigidity from experimental supercoiling data, *Phys. Rev. Lett.* **93**, 198107 1-4 (2004).
- [11] Y. Shi & J.E. Hearst, The Kirchhoff elastic rod, the nonlinear Schrödinger equation, and DNA supercoiling, *J. Chem. Phys.* **101**, 5186-5200 (1994).
- [12] T. Yabuta, N. Yoshizawa & N. Kojima, Cable kink analysis: cable loop stability under tension, *J. Appl. Mech.* **49**, 584-588 (1982).